ARTICLE

Enhanced quantum efficiency from a mosaic of two dimensional MoS_2 formed onto aminosilane functionalised substrates

Yichao Wang,[a] Enrico Della Gaspera,[b,c] Benjamin J. Carey,[a] Paul Atkin,[a,c] Kyle J. Berean,[a] Rhiannon M. Clark,[a,c] Ivan S. Cole,[c] Zai-Quan Xu,[d] Yupeng Zhang,[d] Qiaoliang Bao,[d] Jian Zhen Ou,[a] Torben Daeneke,[a] and Kourosh Kalantar-zadeh[a]

Received 00th January 20xx,
Accepted 00th January 20xx

DOI: 10.1039/x0xx00000x

www.rsc.org/

Developing scalable methods of growing two dimensional molybdenum disulphide (2D MoS_2) of strong optical properties, on any desired substrates, is a necessary step to move towards industrial uptake of this material for optical applications. In this study, Si/SiO_2 substrates were functionalised using self-assembled monolayers of three different aminosilanes with various number of amine groups and molecular lengths, as underlayers for enhancing the adherence of molybdenum precursor. The tetrahedral $[MoS_4]^{2-}$ anion groups from the molybdenum precursor were bonded on these silanised Si/SiO_2 substrates afterwards. The substrates were then treated with a combined thermolysis and sulphurisation step. The results showed that silanisation of the substrates using longest chains and largest number of amine groups provided a good foundation to grow quasi 2D MoS_2 made from adjacent flakes in a mosaic formation. Microscopic and spectroscopic investigations revealed that these quasi 2D MoS_2 formed using this long chain aminosilane resulted in flakes with lateral dimensions in micron and submicron ranges composed of adjoining MoS_2 pieces of 20 to 60 nm in lateral dimensions, dominantly made of 3 to 5 MoS_2 fundamental layers. The obtained quasi 2D MoS_2 shows a high internal quantum efficiency of 2.6% associateed to the quantum confinement effect and high stoichiometry of the adjoining nanoflakes that form the structure of the sheets. The synthesis technique in this study is reliable, facile and offers a procedure to form large, scaleable and patternable quasi 2D MoS_2 sheets on various substrates with enhanced optical properties for practical applications.

Introduction

Two-dimensional (2D) transition metal dichalcogenides (TMDs), and particularly 2D molybdenum disulphide (MoS_2), have attracted great attention in recent years, owing to their unique electronic and optical properties.[1-3]

In comparison to its bulk counterpart, which has an indirect band gap of ~1.3 eV,[4] monolayered MoS_2 has a direct bandgap of ~1.9 eV.[4, 5] Photoluminescence (PL) emission inherited from this direct band gap, make monolayered MoS_2 suitable for many optical units.[6] The high on-off current ratio and good electronic performance exhibited by monolayered MoS_2 transistors suggest their promise in future electronic circuits, requiring low stand-by power attractive for the realisation of 2D optoelectronic devices.[6] To date, 2D MoS_2 has found numerous potentials in units including those incorporated in field-effect transistors (FETs),[7-10] catalysts,[11-16] energy storage,[17, 18] photodetectors,[19] gas separation membranes,[20] piezoelectric systems,[21] bio and gas sensors,[1, 22-26] and photovoltaics.[27] Therefore, synthesis of wafer scale 2D MoS_2 using facile and reliable approaches is essential for widespread application of this material in optical and electronic devices.

In nature, 2H phase of MoS_2 has a stratified crystal. Many top-down techniques such as micromechanical cleavage,[4, 7] liquid exfoliation[28-31] and intercalation-assisted exfoliation[32] have been used for obtaining atomically thin MoS_2 nanoflakes. However, such exfoliation methods are impractical for wafer processes in optical and electronic industries. The yield for mechanical cleavage methods is generally low.[33] Liquid exfoliation always results in laterally polydisperse samples.[28, 29] Many intercalation-assisted exfoliation processes involves the use of hazardous liquids such as butyllithium, which are very reactive and explosive reagents.

The bottom-up techniques are also widely investigated for growing large area MoS_2 thin sheets. They generally rely on the reactions of selected molybdenum-containing compounds on the surface of substrates, together with sulphurisation and

[a] School of Electrical and Computer Engineering, RMIT University, Melbourne, Victoria, Australia.
[b] School of Science, RMIT University, Melbourne, Victoria, Australia
[c] CSIRO Manufacturing Flagship, Clayton, Victoria, Australia
[d] Department of Materials Science and Engineering, Faculty of Engineering, Monash University, Clayton 3800, Victoria, Australia
Email: kourosh.kalantar@rmit.edu.au, jianzhen.ou@rmit.edu.au
Electronic Supplementary Information (ESI) available: Supplementary figures. See DOI: 10.1039/x0xx00000x

annealing steps. For instance, vacuum deposition of Mo,[34] MoO_2 microcrystals,[35] molybdenum trioxide (MoO_3)[6, 36, 37] and $MoCl_5$ powders,[38, 39] followed by sulphurisation processes have been demonstrated. These methods have shown promise in synthesising 2D MoS_2 on substrates such as sapphire,[40] while monolayer of MoS_2 in triangular islands of tens of micrometres in lateral dimensions can be obtained.[6, 37, 41] Many of these reactions normally tend to partially form MoS_2 nanoparticles or nanorod structures during the synthesis and significant tunings are required.[36, 42]

To promote the formation of layered MoS_2, it is common to make use of solution based precursors.[5, 43] These precursors are usually placed on the surface of the substrates using methods such as dip-coating[40] and spin-coating.[4, 41] As one of the first demonstrations on these approaches, Liu *et al.* used a two-step thermolysis process to obtain few-layered MoS_2 thin films.[40] Molybdenum compound was first formed on the substrate and then converted into 2D MoS_2 by annealing and sulphurisation steps. Although the technique leads to high quality MoS_2 thin films, the dip-coating process is not compatible with conventional semiconductor manufacturing practices due to its unsuitability for many large-area applications.[42] Spin-coating is likely to perform worse as it produces uneven thicknesses of the precursor on the wafer.[4]

SiO_2 covered substrates, such as SiO_2/Si, are the most important of all wafers to form 2D MoS_2 onto due to their fundamental significance in electronic and optical device industries. However, so far most of the reports on 2D MoS_2 deposition on SiO_2 have demonstrated lack of localised crystallinity for 2D material's domains due to the relatively high surface roughness and amorphous nature of SiO_2 covered substrates. This leads to reduced optical qualities.[43-45] As such, devising a method that can result in large area 2D MoS_2 with improved and enhanced optical properties, on SiO_2/Si substrates is of great importance.

Many aspects should be considered in the synthesis of 2D MoS_2 with high optical properties. One of the main issues is that 2D MoS_2 has a naturally relatively low internal quantum efficiency which makes it difficult to incorporate in many practical applications in optics. The quantum yield for prototypical 2D MoS_2 has been reported to be less than 1.0%,[46] which results in low optical intensity of light emitting diodes based this material.[46] Also this low quantum yield comes as an obstacle for many bio medical applications in which the readability of the optical signal defines the minimum detection limits.[47] We have previously shown that it is possible to increase the quantum yield by reducing the lateral dimension of MoS_2 nanoflakes in suspensions.[26] Based on this past observation, we hypothesize that if 2D MoS_2 laid on a substrate is made of small adjoining flakes, quantum yield will be enhanced. Creating 2D semiconductors from adjoining flakes may be disadvantageous for making electronic devices but can be of great benefit for developing enhanced optical unit.

One of the approaches that can be potentially used for preparing the surface of substrates for precursors is the use of silane compounds. Silanisation is one of the most used methods for the functionalisation of SiO_2 surface.[48-50]

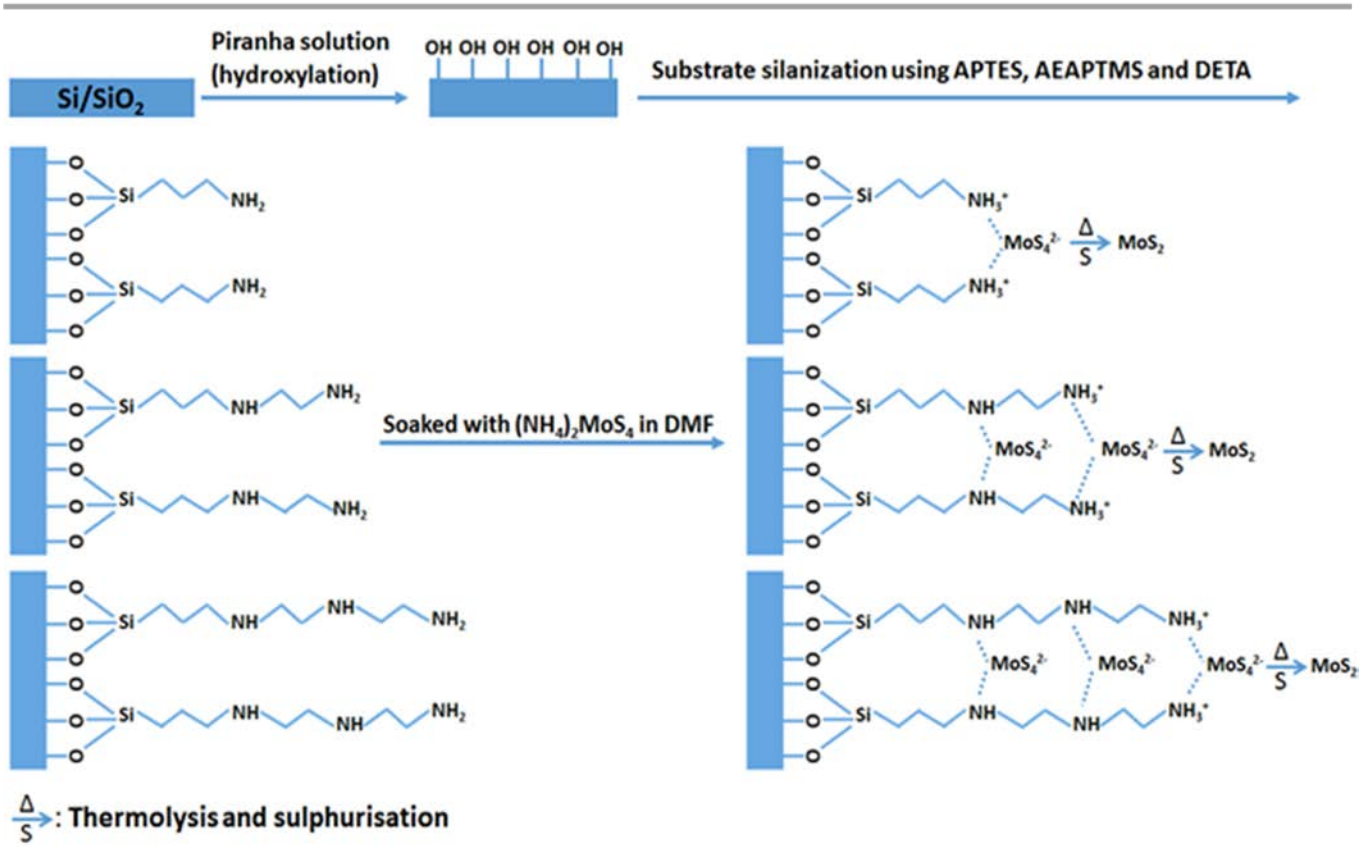

Scheme 1 Si/SiO_2 substrates are cleaned and activated in a piranha solution and modified with APTES, AEAPTMS and DETA. Tetrahedral $[MoS_4]^{2-}$ anion group is bonded on the aminosilane functionalised substrates (only idealised coverage has been shown), after that the substrates are treated through a combined thermolysis and sulphurisation process.

However, the applicability of silanes has not been fully investigated in the deposition of 2D MoS_2 or any other TMDs. Specifically, we are curious to investigate whether the concept of quasi 2D MoS_2, with enhanced optical properties, can be realized using silane based growth. Therefore in this study, we demonstrate the formation of quasi 2D MoS_2, made of adjoining flakes, on silanised Si/SiO_2 substrates using a combined thermolysis and sulphurisation of the attached $[MoS_4]^{2-}$ anion groups. Three different self-assembled monolayers of aminosilane groups of - (3-Aminopropyl)triethoxysilane (APTES), *N*-[3-(Trimethoxysilyl)propyl]ethylenediamine (AEAPTMS) and N^1-(3-Trimethoxysilylpropyl)diethylenetriamine (DETA) are used. These groups have different molecular lengths and amine groups on their backbones. It is shown that DETA, with a longer chain and larger number of the amine group, is the most successful of them in establishing larger size quasi 2D MoS_2 made of small flakes on Si/SiO_2 substrates. To assess the physicochemical properties of the synthesised quasi 2D MoS_2, atomic force microscopy (AFM), X-ray photoelectron spectroscopy (XPS) as well as Raman and PL mapping are conducted. The samples are assessed for their optical properties by measuring the internal quantum efficiency and PL decay dynamics.

Results and discussions

Quasi 2D MoS_2 flakes were formed on Si/SiO_2 substrates *via* thermolysis and sulphurisation after the substrates are silanised using three different aminosilanes. Details are presented in the Methods section. In brief, the Si/SiO_2 substrates were cleaned and hydroxylated in a piranha solution. After that the wafers were immersed in freshly prepared APTES, AEAPTMS and DETA solutions in ethanol. Then the substrates were soaked in a solution-phase precursor of $(NH_4)_2MoS_4$ in dimethylformamide (DMF). In the following step, the samples were treated using a thermolysis and sulphurisation process. The synthesis process is illustrated in Scheme 1.

The interaction between amine groups of aminosilane and $(NH_4)_2MoS_4$ is described by:

$$2\,(R\text{-}NH_2)+(NH_4)_2MoS_4 \rightarrow 2\,(R\text{-}NH_3)MoS_4+2NH_3\uparrow \qquad (1)$$

in which R is all the structure of aminosilane without one NH_2 functional group. The formula is based on the acid-base reaction between aminosilanes and $(NH_4)_2MoS_4$. Here, NH_3 as a weaker base can be released and was removed in the vacuum oven. This leads to a shift of the reaction equilibrium and tetrahedral $[MoS_4]^{2-}$ anion group non-reversible interaction on the substrate. The same principle has been illustrated for the reaction of $(NH_4)_2MoS_4$ with ethylenediamine to obtain the diammonium salt.[51]

The control of surface wettability *via* functional groups plays an important role in study of the surface and ion exchange properties.[52] As a result, water contact angle (WCA) measurements were conducted on the piranha treated and three different silanised Si/SiO_2 substrates. The piranha treated Si/SiO_2 substrate shows strong hydrophilicity (Fig. 1a), resulting in a WCA value of $23.5^o \pm 0.8^o$. This is due to the appearance of OH group on the surface. After treated with the piranha solution, the cross-linked Si-O bond on SiO_2 surface were oxidised and hydroxylated by hydrogen peroxide (H_2O_2) and ammonium hydroxide (NH_4OH). After the silanisation, aminosilanes of APTES, AEAPTMS and DETA in this

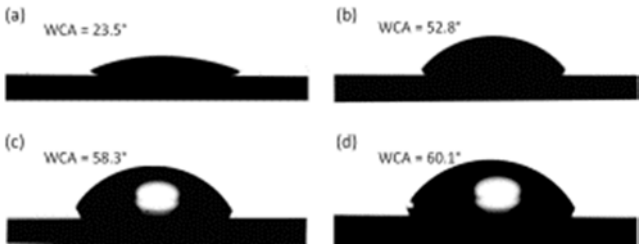

Fig. 1 WCA measurements performed on (a) piranha treated Si/SiO_2 substrate and on Si/SiO_2 substrates modified with: (b) APTES, (c) AEAPTMS, and (d) DETA.

study, with their alky chains, ethoxyl and amine groups appear on the surface. In these cases, the WCA increased to $52.8^o \pm 0.5^o$, $58.3^o \pm 0.2^o$ and $60.1^o \pm 0.8^o$, for APTES, AEAPTMS and DETA, respectively (Fig. 1b-d). This corresponds to an increasingly higher WCA and reduction in the degree of hydrophilicity, indicating that the longer DETA chain resulted in a larger contact angle. The larger contact angle is likely to promote the precursor reaction on the surface of the substrate, which is beneficial for obtaining larger size quasi 2D MoS_2 flakes.

Silanisation process provides amine groups on Si/SiO_2 surface which facilitates the $[MoS_4]^{2-}$ anion interaction. After the substrates were treated using thermolysis and sulphurisation, quasi 2D MoS_2 nanoflakes were formed. AFM was used for characterising the surface morphology and thickness of quasi 2D MoS_2. The topographic images and corresponding height profiles for the obtained flakes are presented in Fig. 2a-c.

As can be seen from Fig. 2a, the nanoflakes synthesised on APTES silanised substrates have lateral dimensions in the order of ~100 nm and are sparsely located on the substrate. Clear steps of ~3–4 nm (corresponding to ~4–6 monolayers of MoS_2 - thickness of monolayer MoS_2 is 0.65 nm) can be observed in typical nanoflakes. For the MoS_2 grown on an AEAPTMS silanised substrate, larger flakes begin to appear. The lateral dimensions are increased to ~350 nm and thicknesses of the flakes are between 3 and 5 nm (Fig. 2b). From the AFM images, it is revealed that the DETA silanised substrate provides the best platform to grow the largest quasi 2D MoS_2 nanosheets. From the example presented in Fig. 2c, it is seen that the obtained nanoflakes had a thickness of ~2-3 nm, which corresponds to ~3 to 5 MoS_2 monolayers. DETA has more bonding sites which has larger number of $-NH_2$ groups. It was also shown that DETA makes the largest WCA. As a result, $[MoS_4]^{2-}$ groups have more possible affinity sites and highest probability to come close and interact with the DETA silanised substrate (Scheme 1), compared to APTES and AEAPTMS treated surfaces, leading to a larger dimension of quasi 2D MoS_2 nanoflakes. In our large samples, the surface roughness (σ) was measured using AFM. The surface roughness of the bare Si/SiO_2, DETA silanised, and MoS_2 grown on DETA silanised substrates were measured and compared with the background roughness. From the analysis, the root mean square (RMS) surface roughness for the DETA silanised sample and its background SiO_2/Si substrate was found to be ~400 and 130 pm, respectively, confirming that surface functionalization led to a jagged surface and possibly made of smaller adjoining connected flakes. The other important observation is the fact that jagged 2D MoS_2 formed on DETA silanised substrates are made of adjoining small flakes of ~30-50 nm (as an example Fig. 2d). The schematic map which presents the formation of this unique 2D structure is

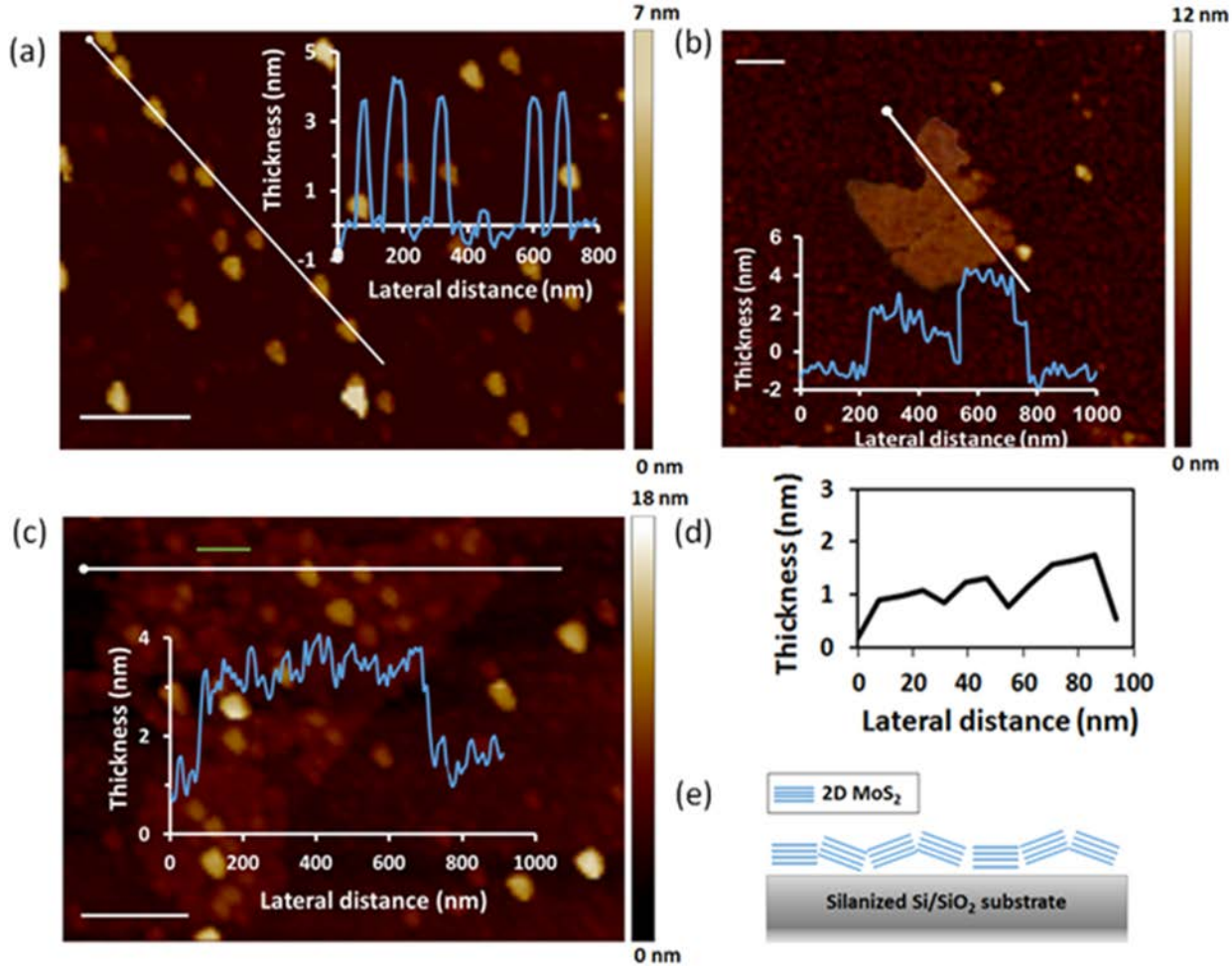

Fig. 2 AFM images and height profiles of 2D MoS_2 nanoflakes synthesised on: (a) APTES, (b) AEAPTMS and (c) DETA silanised Si/SiO_2 substrates. Scale bars represent 200 nm. (d) Height profile along the green line overlaid in image (c). (e) Schematic cross sectional representation of the quasi 2D MoS_2 sheet made of adjoining small flakes.

shown in Fig. 2e. It seems that DETA molecules are assembled at different angles on the substrates. Different angles mean various heights for the MoS_2 growth points with reference to the substrate's surface. This, in result, promotes the formation of jagged and adjoining 2D surfaces of MoS_2.

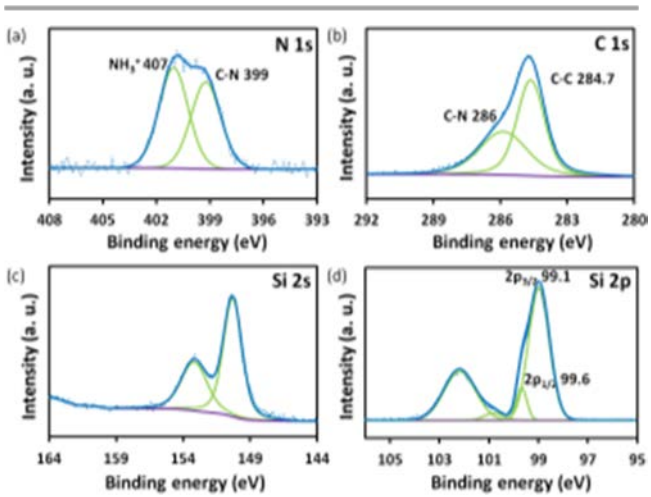

Fig. 3 XPS spectra of (a) N 1s, (b) C 1s, (c) Si 2p, and (d) Si 2s binding energies from the DETA silanised substrate.

As in this study DETA produced the largest quasi 2D MoS_2 flakes, the optical and compositional analysis will be more comprehensively presented based on this self-assembled monolayer.

XPS was used for determining the chemical compositions and chemical states of the DETA monolayers and obtained quasi 2D MoS_2 sheets. Before we carried out studies on the $[MoS_4]^{2-}$ anion surface treated samples, as a control experiment, the DETA treated substrates were first investigated by XPS to ensure that all the expected elements of the aminosilane are on the surface. For the DETA silanised substrate, two peaks are seen in the N 1s spectra, one at 399 eV binding energy related to the C-N binding and the other at 407 eV due to the protonated amines (Fig. 3a).[53, 54] The deconvoluted C 1s spectrum shows two peaks with binding energy of 284.7 and 286 eV, which are ascribed to C-C and C-N bondings (Fig. 3b).[53, 54] Si 2s has the same peak locations as a previous study (Fig. 3c).[54] For the spectra of Si 2p peak (Fig. 3d), it shows two binding energies at 99.1 and 99.6 eV, corresponding to Si $2p_{3/2}$ and Si $2p_{1/2}$ from the bulk silicon wafer beneath the oxide layer.[53] The

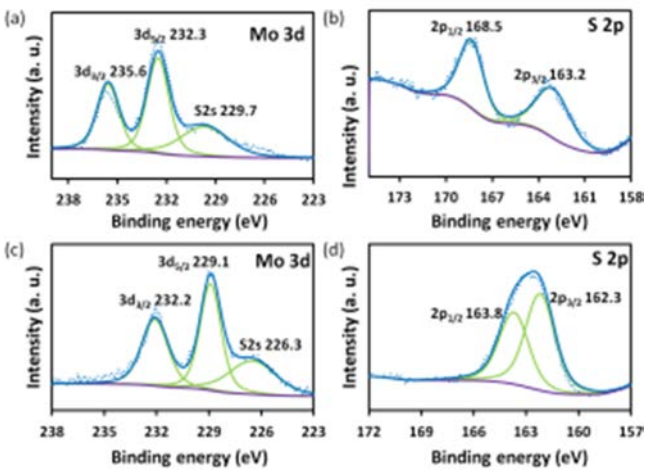

Fig. 4 XPS spectra of (a) Mo 3d and (b) S 2p binding energies from substrate with molybdenum precursor after DETA silanisation. (c) and (d) are the aforementioned elements binding energies of the samples after the combined thermolysis and sulphurisation process.

signal appears at the binding energy of 100.9 eV is contributed by aminosilane (Si-O) on the silicon dioxide and the one at 102.2 eV is ascribed to silicon dioxide.[53]

For the DETA silanised substrates with the molybdenum precursor, the XPS results for Mo and S binding energies are shown in Fig. 4a and 4b. The deconvoluted Mo 3d spectrum shows that two Mo 3d peaks at 232.3 and 235.6 eV, corresponding to the $3d_{3/2}$ and $3d_{5/2}$ binding energies, respectively, characteristic for the Mo^{6+} state.[4] The S 2s peak can be observed at 229.7 eV. From S 2p spectra, S $2p_{1/2}$ and S $2p_{3/2}$ are located at 168.5 and 163.2 eV (Fig. 4b). The XPS assessments provide good evidence that the DETA silanisation process has been a success.

After the substrates were treated with a combined thermolysis and sulphurisation, obtained quasi 2D MoS_2 flakes were observed to have lower binding energies for Mo 3d and S 2p peaks (Fig. 4c and d). It also exhibited two characteristic Mo 3d peaks at 229.1 and 232.2 eV, corresponding to the $3d_{3/2}$ and $3d_{5/2}$ binding energies for Mo^{4+}.[29] S 2s peak was found at 226.3 eV. The sulphur peak for the 2p orbital (Fig. 4b and d) is shifted from 163.2 to 162.3 eV (for $2p_{3/2}$) and from 168.5 to 163.8 eV (for $2p_{1/2}$). Decreases of binding energy for both Mo and S elements are due to the change of oxidation state of Mo from Mo^{6+} to Mo^{4+}, which leads to a reduction of bonding strength between Mo and S. The XPS results confirm the Mo oxidation transition from +6 to +4, which means the transition from bonded $[MoS_4]^{2-}$ anion groups to nearly perfect stoichiometric MoS_2 composition after the thermolysis and sulphurisation process.

The XPS results for MoS_2 grown on APTES and AEAPTMS silanised substrate were also confirmed to form MoS_2. The data are presented in the Supporting Information.

Energy dispersive X-ray (EDX) spectrum measurement was used for characterising the chemical composition of the synthesised MoS_2 nanosheets and the result is shown in Figure S3. Peaks associated with Mo and S are found at 2.29 and 2.3 keV in the spectrum. Quantitative analysis shows that the atomic ratio of S to Mo is approximately 2.1, which further confirms stoichiometric state of MoS_2.

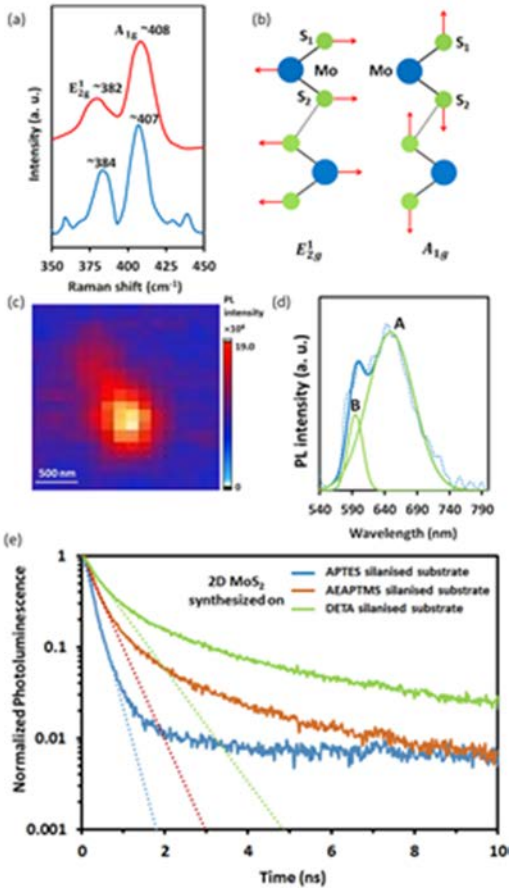

Fig. 5 (a) Raman spectra of DETA salinised samples on the Si/SiO_2 substrate. (b) Schematics of $\mathbf{E^1_{2g}}$ and $\mathbf{A_{1g}}$ Raman vibrational modes. (c) PL mapping image showing the integrated intensities of A and B exciton peaks. (d) Typical PL spectrum extracted of a sample. (e) PL decay graphs with fitted exponential of three APTES, AEAPTMS and DETA samples for comparison.

Raman spectroscopy is also used for assessing the thickness and number of layers of the obtained quasi 2D MoS_2 flakes on DETA silanised Si/SiO_2 substrate. From Fig. 5a, the spectrum reveals that two characteristic Raman modes of MoS_2, $\mathbf{E^1_{2g}}$ and $\mathbf{A_{1g}}$, which represents the in-plane strain and out-of-plane modes (Fig. 5b). The frequency difference between $\mathbf{E^1_{2g}}$ and $\mathbf{A_{1g}}$ phonons has been shown as an indicator of the number of the layers in MoS_2.[55] We observe the frequency difference of the $\mathbf{E^1_{2g}}$ and $\mathbf{A_{1g}}$ peaks in different sample areas to be around 23 to 26 cm^{-1}. The Raman spectra results indicate that 3 to 5 layers can be dominant in different regions of the synthesised flakes.[40] This Raman spectroscopy results are also consistent with the AFM profiles.

MoS_2 nanosheets synthesised in this method have a polycrystalline structure. This can be evidenced in a full range scan of Raman spectroscopy. From Figure S4, Raman spectra at 520 and 300 cm^{-1} are contributed by Si/SiO_2 substrate. Two MoS_2 Raman modes are located at 407 and 384 cm^{-1}. Interestingly, there is an additional peak at 226 cm^{-1} which is suggested to be a disordered-induced peak ascribed to MoS_2 due to first-order scattering of LA(M) phonons obtained from randomly oriented MoS_2.[44] Besides this, AFM image in Figure 2 of the manuscript also shows that MoS_2 sheets are composed of adjoining small nanoflakes with different

orientations. This can further confirm that the synthesised MoS_2 nanosheets in this study have a polycrystalline nature.

X-ray diffraction (XRD) was also conducted for the as grown MoS_2 flakes and the result is presented in Figure S5. From the XRD pattern, the typical planar MoS_2 peak at 14.5° which corresponds to (002) plane was not observed, confirming the polycrystalline nature of our quasi 2D MoS_2 sheets.

PL measurements: To investigate the optical properties of the quasi 2D MoS_2 flakes made of adjacent entities in a mosaic formation, PL mapping was performed. PL spectroscopy was also conducted to explore whether the formation of the small flakes cause any improvement in the PL signatures. Fig. 5c shows the PL intensity-integrated map and the average PL spectrum obtained from the region plotted in Fig. 5d.

Using the Fityk Software package (version 0.9.2), two Gaussian curves were estimated to fit the obtained PL spectrum. These two peaks are at 590 and 650 nm, which correspond to the energy of the B and A excitons in quasi 2D MoS_2. Blue shifting of the PL emission peak was observed compared to the previous report on 2D MoS_2 deposited on glass substrates.[56] The shift can be due to the combination of two different effects. It may be due to the suppression of A excition in *n*-type doped MoS_2 by the Si/SiO_2 substrate, resulting in only A^- (trion) contributing to PL.[57] Excitons are generated when photons, with sufficient energy, excite semiconductors like 2D MoS_2. These excitons are electron-hole pairs which are attracted to each other by coulomb forces. These forces become more prominent when the thickness of the thin film decreases. Therefore, nanoflakes with relatively small dimensions contribute to higher energy PL emission.[58] The shift can also be due to the quantum confinement effect associated to the small dimensions of the adjacent flakes forming the main planes. This observation was also similarly seen in the liquid phase 2D MoS_2 with laterally polydispersed samples.[19, 26]

To compare the photodynamics of our synthesised quasi 2D MoS_2 with previous works, we assess the internal quantum efficiencies of the samples. Internal quantum efficiency η_i is obtained using the following equations:[59]

$$\eta_i = \frac{\mathrm{Bn}^2}{\mathrm{G}} \tag{2}$$

$$\mathrm{I_{PL}} = \theta \mathrm{Bn}^2 \tag{3}$$

$$\mathrm{G} = \frac{0.4 \times \mathrm{P_{laser}} \alpha}{\mathrm{A_{spot}} h\nu} \tag{4}$$

Here B represents the radiative bimolecular coefficient, n is the photoexcited carrier concentration, and G is the steady state carrier generation/recombination rate, which is calculated using the experimental equation (4). In equation (3), θ is a constant which can be determined based on the measurement parameters presented in ref 50 and $\mathrm{I_{PL}}$ is the integrated PL intensity. In equation (4), $\mathrm{P_{laser}}$, $\mathrm{A_{spot}}$, and $h\nu$ are the laser power, excitation area, and excitation photon energy, respectively, and $\boldsymbol{\alpha}$ is ~0.05 per layer. [59]

Total lateral dimensions of quasi 2D MoS_2 planes sufficiently large to ensure the illumination of the entire nanosheet by the laser for the DETA silanised sample, allowing the determination of the quantum yield. The calculated internal quantum efficiency of our 3~5 layered sample is found to be 2.6%, which is possibly indicative of a highly stoichiometry sample. This is associated with theoretical mono layer efficiency of ~11%. Non-radiative recombination processes frequently occur at defect sites and thus the quantum yield can be utilised to assess the degree of stoichiometry. In comparison to our result, high quality mechanically exfoliated monolayer MoS_2 flakes feature an intrinsic internal quantum efficiency of 8.3% at room temperature for one layer.[59] The highest observed internal quantum efficiency for monolayer MoS_2 has been reported to be above 95%.[46] To achieve this high efficiency, Amani *et. al.* designed a process to functionalise mechanically exfoliated flakes using the nonoxidising organic superacid bis(trifluoromethane) sulfonimide. This kind of superacid successfully inhibited defect-mediated nonradiative recombination processes, leading to the largely increased quantum efficiency.[46] The internal quantum efficiency obtained from ion intercalation-assisted exfoliated monolayer MoS_2 flakes has been reported to be 1.3%,[60] which is less than that of our samples.

The enhancement of internal quantum efficiency may also be due to quantum confinement effects due to the formation of a mosaic of smaller flakes within the structure of quasi 2D MoS_2. It has been reported the quantum efficiency increases with decreasing of flake sizes, as smaller size of samples lead to fewer nonradioactive recombination.[61] The idea has been extended to 2D flakes with small lateral dimensions, generating quantum confinement within thickness and across.[19, 26] As a result, the presence of small flakes may result from an increase of internal quantum efficiency. For our samples, as can be seen from Fig. 2c and d, the synthesised sheets have a mosaic structure, which is composed of adjoining small MoS_2 nanoflakes.

PL radiative decay of quasi 2D MoS_2 grown on three different silanised substrates was also measured in this study. Fitting of the data in Figure 5e, the mean excitonic recombination time for quasi 2D MoS_2 grown on APTES, AEAPTMS and DETA were determined to be 0.26, 0.43 and 0.70 ns. Considering that the DETA sample provides the longest recombination time, the assumption that it has the lowest defect and hence a relatively large internal quantum efficiency is confirmed.

All in all, the technique presented in this paper, when further perfected, can be potentially used as a replacement to CVD methods for the deposition of specific configurations of 2D MoS_2. Advantageously, the as grown layers can also take the shape of patterns on pre-silanised substrates. The method is also compatible with other liquid phase deposition techniques. This method can be transferrable to grow other TMD nanosheets. The reaction in this study is based on the interaction between amine groups of aminosilane and transition metal containing precursor in the form of ammonium salt. TMD nanosheets can be obtained via a combined thermolysis and sulphurisation of the transition metal precursor on silanised Si/SiO_2 substrate.

Materials and Methods

The Si-SiO_2 wafers (<100>, n-doped, 0-100 Ω cm, 300 nm-thick dry thermal grown silicon dioxide) were purchased from WRS Materials (San Jose, CA, USA). APTES, AEAPTMS and DETA were purchased from Sigma Aldrich. Ammonium tetrathiomolybdate ($(NH_4)_2MoS_4$) was ordered from Sigma. Toluene and Dimethylformamide (DMF) was purchased from Sigma. DI water was used throughout the experiment.

Surface functionalisation of Si/SiO_2 substrate with aminosilanes

The Si-SiO_2 wafers were cut into 10×10 mm^2 pieces. The substrates were sequentially cleaned with acetone and 2-propanol in an ultrasonic bath for 3 minutes, respectively, followed by rinsing with DI water and then dried with N_2 flow. The substrate 300 nm SiO_2 on Si (SiO_2/Si) was first cleaned with a standard piranha solution (a mixture of 3:1 (v/v) 30% H_2O_2 and 27% NH_4OH) at 70 ℃ for 30 min. The substrate was functionalised with APTES, AEAPTMS and DETA using the method reported previously.[50] Briefly, self-assembled monolayers of aminosilanes on Si/SiO_2 substrates with $-NH_2$ functional groups were prepared by soaking the substrates in a 2% solution of APTES, AEAPTMS and DETA in ethanol for 30 mins. Upon their removal from the solution, the samples were washed thoroughly with ethanol and then blown dry with nitrogen.

Surface attachment of the Mo containing ions on substrates

0.15 g of high purity of $(NH_4)_2MoS_4$ powder was added to 20 mL of DMF solvent to form a solution. The concentration was chosen based on the suggestion by Liu et al.[43] The solution was sonicated in a bath sonicator for 10 mins to obtain a homogeneous solution. The silanised substrates were soaked in the aforementioned prepared solution for one hour. This time was chosen as it provided the best coverage on the surface of the substrates, which was inspected under an optical microscope and was based according to the overall change of colour. DFM was used for rinsing before the samples were blown dry with a flow of N_2.

Thermolysis process by annealing and sulphurisation

After soaking, the substrates were immediately moved into a chemical vapour deposition (CVD) furnace in which the sulphur powder was placed in the colder zone at 300°C and sample substrates were placed on the reaction zone of the quartz tube and kept at 450 °C. The forming gas was a static gas mixture of Ar and H_2 (95:5, vol/vol).

Characterisation of silanised substrate and grown MoS_2 thin films

AFM (Bruker Dimension Icon) in a tapping mode was used for assessing the thickness and topology of the flakes and images were analysed using Scan-assist® Software. Raman spectra were obtained using a confocal microscope system (WITec, alpha 300R) with a ×100 objective (NA = 0.9) in an ambient condition. A 532 nm laser was used to excite samples which were placed on a piezo crystal-controlled scanning state. XPS measurements were performed on a Thermo scientific K-Alpha VG-310F instrument using aluminium monochromated X-rays (20 kV, 15 mA) with the hemispherical energy analyser set at a pass energy of 20 eV for the peak scans. WCA measurements were conducted using an OCA 20 system (DataPhysics Instruments, GmbH, Germany) with an automatic dispenser. The height of the each drop was confirmed using a CCD camera prior to each measurement to ensure consistency in the drop volume. A 10 µL DI water droplet was dropped on the surface of the gel and the angle is measured using the circle fit. The PL mapping was carried out on a custom build instrument using a Quantum GEM 532 nm and a Fianium WhiteLase (WL-SC400-8 – 405 nm) laser for excitation delivering 350 µW of laser light at the sample position. A Nikon air objective (100×0.9 NA), in combination with a 532 nm (or 405 nm) notch filter, was used.

Conclusions

In summary, we demonstrated the synthesis of large-area quasi 2D MoS_2 nanosheets, made of adjoining flakes, by the aminosilane functionalisation and subsequent thermolysis and sulphurisation of Si/SiO_2 substrates. AFM results show that samples obtained from the DETA functionalisation provided the best foundation to grow relatively large quasi 2D MoS_2 sheets. The characterisation of these thin sheets showed that lateral dimensions in the order of micron or submicron and dominant 3-5 layers were obtained, which are made of nanoflakes with the lateral dimensions in the order of 30 to 50 nm. The number of layers was also confirmed by Raman spectroscopy.

The surface contact angle measurements showed that the lowest wettability belonged to DETA covered substrates. This observation together with the fact that DETA has the longest chain and larger number of amine groups on its chain were associated to the more efficient lateral growth of quasi 2D MoS_2 sheets on SiO_2 substrate. XPS confirmed the formation of highly stoichiometric 2D MoS_2, which was also confirmed by PL decay assessments.

The obtained quasi 2D MoS_2 nanosheets sheets using DETA functionalised substrates had a high internal quantum efficiency and relatively long excitonic recombination time, which were associated to the quantum confinement effect in the mosaic of adjoining small nanoflakes and also the high stoichiometry of the 2D material.

This work presents a new approach for depositing quasi 2D MoS_2 sheet with enhanced optical properties by an intermediate process of silanisation which is particularly compatible with oxide surfaces.

Acknowledgements

The authors would like to acknowledge the facilities, scientific and technical assistances of the Australian Microscopy and Microanalysis Research Facility (AMMRF) and the Micro Nano Research Facility (MNRF) at RMIT. They also acknowledge help from the Australian Centre for Materials Science and Engineering (CMSE) of the Commonwealth Scientific and Industrial Research Organisation (CSIRO), Australia. The research was financially supported by the Australian Research Council (ARC) through Discovery Project DP140100170. Q. Bao would like to acknowledge the support from ARC DECRA DE120101569 and Discovery Project DP140101501.

References

37 S. Wu, C. Huang, G. Aivazian, J. S. Ross, D. H. Cobden and X. Xu, *ACS Nano*, 2013, **7**, 2768-2772.

38 A. M. van der Zande, P. Y. Huang, D. A. Chenet, T. C. Berkelbach, Y. You, G.-H. Lee, T. F. Heinz, D. R. Reichman, D. A. Muller and J. C. Hone, *Nat. Mater.*, 2013, **12**, 554-561.

39 X. L. Li and Y. D. Li, *Chem–Eur. J.*, 2003, **9**, 2726-2731.

40 K.-K. Liu, W. Zhang, Y.-H. Lee, Y.-C. Lin, M.-T. Chang, C.-Y. Su, C.-S. Chang, H. Li, Y. Shi, H. Zhang, C.-S. Lai and L.-J. Li, *Nano. Lett.*, 2012, **12**, 1538-1544.

41 J.-M. Yun, Y.-J. Noh, J.-S. Yeo, Y.-J. Go, S.-I. Na, H.-G. Jeong, J. Kim, S. Lee, S.-S. Kim, H. Y. Koo, T.-W. Kim and D.-Y. Kim, *J. Mater. Chem. C*, 2013, **1**, 3777-3783.

42 J. Yang, Y. Gu, E. Lee, H. Lee, S. H. Park, M.-H. Cho, Y. H. Kim, Y.-H. Kim and H. Kim, *Nanoscale*, 2015, **7**, 9311-9319.

43 D. Dumcenco, D. Ovchinnikov, K. Marinov, P. Lazić, M. Gibertini, N. Marzari, O. L. Sanchez, Y.-C. Kung, D.

Krasnozhon, M.-W. Chen, S. Bertolazzi, P. Gillet, A. Fontcuberta i Morral, A. Radenovic and A. Kis, *ACS Nano*, 2015, **9**, 4611-4620.
44 S. Najmaei, M. Amani, M. L. Chin, Z. Liu, A. G. Birdwell, T. P. O'Regan, P. M. Ajayan, M. Dubey and J. Lou, *ACS Nano*, 2014, **8**, 7930-7937.
45 O. V. Yazyev and Y. P. Chen, *Nat. Nanotechnol*, 2014, **9**, 755-767.
46 M. Amani, D.-H. Lien, D. Kiriya, J. Xiao, A. Azcatl, J. Noh, S. R. Madhvapathy, R. Addou, S. KC, M. Dubey, K. Cho, R. M. Wallace, S.-C. Lee, J.-H. He, J. W. Ager, X. Zhang, E. Yablonovitch and A. Javey, *Science*, 2015, **350**, 1065-1068.
47 K. Aslan, I. Gryczynski, J. Malicka, E. Matveeva, J. R. Lakowicz and C. D. Geddes, *Curr. Opin. Biotech.*, 2005, **16**, 55-62.
48 R. Tian, O. Seitz, M. Li, W. Hu, Y. J. Chabal and J. Gao, *Langmuir*, 2010, **26**, 4563-4566.
49 A. V. Krasnoslobodtsev and S. N. Smirnov, *Langmuir*, 2002, **18**, 3181-3184.
50 J. A. Howarter and J. P. Youngblood, *Langmuir*, 2006, **22**, 11142-11147.
51 J. Pütz, PhD Thesis, Saarland University, 2000.
52 O. Gonzalez-Ortega and R. Guzman, *American J. Anal. Chem.*, 2014, **5**, 932-944.
53 G. Jakša, B. Štefane and J. Kovač, *Surf. Interface Anal.*, 2013, **45**, 1709-1713.
54 Y. Wang, M. Lieberman, Q. Hang and G. Bernstein, *Int. J. Mol. Sci.*, 2009, **10**, 533-558.
55 H. Li, Q. Zhang, C. C. R. Yap, B. K. Tay, T. H. T. Edwin, A. Olivier and D. Baillargeat, *Adv. Funct. Mater.*, 2012, **22**, 1385-1390.
56 K. P. Dhakal, D. L. Duong, J. Lee, H. Nam, M. Kim, M. Kan, Y. H. Lee and J. Kim, *Nanoscale*, 2014, **6**, 13028-13035.
57 N. Scheuschner, O. Ochedowski, A.-M. Kaulitz, R. Gillen, M. Schleberger and J. Maultzsch, *Phys. Rev. B*, 2014, **89**, 125406.
58 G. W. Mudd, S. A. Svatek, T. Ren, A. Patanè, O. Makarovsky, L. Eaves, P. H. Beton, Z. D. Kovalyuk, G. V. Lashkarev, Z. R. Kudrynskyi and A. I. Dmitriev, *Adv. Mater.*, 2013, **25**, 5714-5718.
59 O. Salehzadeh, N. H. Tran, X. Liu, I. Shih and Z. Mi, *Nano Lett.*, 2014, **14**, 4125-4130.
60 H. D. Ha, D. J. Han, J. S. Choi, M. Park and T. S. Seo, *Small*, 2014, **10**, 3858-3862.
61 N. F. Borrelli, D. W. Hall, H. J. Holland and D. W. Smith, *J. Appl. Phys.*, 1987, **61**, 5399-5409.

1 1. K. Kalantar-zadeh, J. Z. Ou, T. Daeneke, M. S. Strano, M. Pumera and S. L. Gras, *Advanced Functional Materials*, 2015, **25**, 5086-5099.
2 2. M. Chhowalla, H. S. Shin, G. Eda, L.-J. Li, K. P. Loh and H. Zhang, *Nat Chem*, 2013, **5**, 263-275.
3 3. C. Tan and H. Zhang, *Chemical Society Reviews*, 2015, **44**, 2713-2731.
4 4. K. F. Mak, C. Lee, J. Hone, J. Shan and T. F. Heinz, *Phys. Rev. Lett.*, 2010, **105**, 136805.
5 5. A. S. George, Z. Mutlu, R. Ionescu, R. J. Wu, J. S. Jeong, H. H. Bay, Y. Chai, K. A. Mkhoyan, M. Ozkan and C. S. Ozkan, *Advanced Functional Materials*, 2014, **24**, 7461-7466.
6 6. Y.-H. Lee, X.-Q. Zhang, W. Zhang, M.-T. Chang, C.-T. Lin, K.-D. Chang, Y.-C. Yu, J. T.-W. Wang, C.-S. Chang, L.-J. Li and T.-W. Lin, *Advanced Materials*, 2012, **24**, 2320-2325.
7 7. B. Radisavljevic, A. Radenovic, J. Brivio, V. Giacometti and A. Kis, *Nat. Nanotechnol.*, 2011, **6**, 147-150.
8 8. B. Liu, L. Chen, G. Liu, A. N. Abbas, M. Fathi and C. Zhou, *ACS Nano*, 2014, **8**, 5304-5314.
9 9. Y. Che, Y.-C. Lin, P. Kim and C. Zhou, *ACS Nano*, 2013, **7**, 4343-4350.
10 10. H. Li, Z. Yin, Q. He, H. Li, X. Huang, G. Lu, D. W. H. Fam, A. I. Y. Tok, Q. Zhang and H. Zhang, *Small*, 2012, **8**, 63-67.
11 11. A. Ambrosi, X. Chia, Z. Sofer and M. Pumera, *Electrochemistry Communications*, 2015, **54**, 36-40.
12 12. M. Z. M. Nasir, Z. Sofer, A. Ambrosi and M. Pumera, *Nanoscale*, 2015, **7**, 3126-3129.
13 13. Y. Wang, B. J. Carey, W. Zhang, A. F. Chrimes, L. Chen, K. Kalantar-zadeh, J. Z. Ou and T. Daeneke, *The Journal of Physical Chemistry C*, 2016, **120**, 2447–2455.
14 14. S. M. Tan and M. Pumera, *ACS Applied Materials & Interfaces*, 2016, **8**, 3948-3957.
15 15. Z. He and W. Que, *Applied Materials Today*, 2016, **3**, 23-56.
16 16. X. Chia, A. Y. S. Eng, A. Ambrosi, S. M. Tan and M. Pumera, *Chemical Reviews*, 2015, **115**, 11941-11966.
17 17. Q. Weng, X. Wang, X. Wang, C. Zhang, X. Jiang, Y. Bando and D. Golberg, *J. Mater. Chem. A*, 2015, **3**, 3097-3102.
18 18. J.-Z. Wang, L. Lu, M. Lotya, J. N. Coleman, S.-L. Chou, H.-K. Liu, A. I. Minett and J. Chen, *Adv. Energy Mater.*, 2013, **3**, 798-805.
19 19. O. Lopez-Sanchez, D. Lembke, M. Kayci, A. Radenovic and A. Kis, *Nat. Nanotechnol.*, 2013, **8**, 497-501.
20 20. K. J. Berean, J. Z. Ou, T. Daeneke, B. J. Carey, E. P. Nguyen, Y. Wang, S. P. Russo, R. B. Kaner and K. Kalantar-zadeh, *Small*, 2015, **11**, 5035-5040.
21 21. W. Wu, L. Wang, Y. Li, F. Zhang, L. Lin, S. Niu, D. Chenet, X. Zhang, Y. Hao, T. F. Heinz, J. Hone and Z. L. Wang, *Nature*, 2014, **514**, 470-474.
22 22. J. Z. Ou, A. F. Chrimes, Y. Wang, S. Y. Tang, M. S. Strano and K. Kalantar-zadeh, *Nano Letters*, 2014, **14**, 857-863.
23 23. Q. He, Z. Zeng, Z. Yin, H. Li, S. Wu, X. Huang and H. Zhang, *Small*, 2012, **8**, 2994-2999.
24 24. C. Zhu, Z. Zeng, H. Li, F. Li, C. Fan and H. Zhang, *J. Am. Chem. Soc.*, 2013, **135**, 5998-6001.
25 25. K. Kalantar-zadeh and J. Z. Ou, *ACS Sensors*, 2015, DOI: 10.1021/acssensors.5b00142.
26 26. A. H. Loo, A. Bonanni, A. Ambrosi and M. Pumera, *Nanoscale*, 2014, **6**, 11971-11975.
27 27. S. Wi, H. Kim, M. Chen, H. Nam, L. J. Guo, E. Meyhofer and X. Liang, *ACS Nano*, 2014, **8**, 5270-5281.
28 28. J. N. Coleman, M. Lotya, A. O'Neill, S. D. Bergin, P. J. King, U. Khan, K. Young, A. Gaucher, S. De, R. J. Smith, I.

V. Shvets, S. K. Arora, G. Stanton, H.-Y. Kim, K. Lee, G. T. Kim, G. S. Duesberg, T. Hallam, J. J. Boland, J. J. Wang, J. F. Donegan, J. C. Grunlan, G. Moriarty, A. Shmeliov, R. J. Nicholls, J. M. Perkins, E. M. Grieveson, K. Theuwissen, D. W. McComb, P. D. Nellist and V. Nicolosi, *Science*, 2011, **331**, 568-571.

29 29. Y. Wang, J. Z. Ou, S. Balendhran, A. F. Chrimes, M. Mortazavi, D. D. Yao, M. R. Field, K. Latham, V. Bansal, J. R. Friend, S. Zhuiykov, N. V. Medhekar, M. S. Strano and K. Kalantar-zadeh, *ACS Nano*, 2013, **7**, 10083-10093.

30 30. Y. Wang, J. Z. Ou, A. F. Chrimes, B. J. Carey, T. Daeneke, M. M. Y. A. Alsaif, M. Mortazavi, S. Zhuiykov, N. Medhekar, M. Bhaskaran, J. R. Friend, M. S. Strano and K. Kalantar-Zadeh, *Nano Letters*, 2015, **15**, 883–890.

31 31. E. P. Nguyen, B. J. Carey, J. Z. Ou, J. van Embden, E. D. Gaspera, A. F. Chrimes, M. J. S. Spencer, S. Zhuiykov, K. Kalantar-zadeh and T. Daeneke, *Advanced Materials*, 2015, **27**, 6225-6229.

32 32. G. Eda, H. Yamaguchi, D. Voiry, T. Fujita, M. Chen and M. Chhowalla, *Nano Lett.*, 2011, **11**, 5111-5116.

33 33. F. Bonaccorso, A. Lombardo, T. Hasan, Z. Sun, L. Colombo and A. C. Ferrari, *Materials Today*, 2012, **15**, 564-589.

34 34. Y. Zhan, Z. Liu, S. Najmaei, P. M. Ajayan and J. Lou, *Small*, 2012, **8**, 966-971.

35 35. X. Wang, H. Feng, Y. Wu and L. Jiao, *Journal of the American Chemical Society*, 2013, **135**, 5304-5307.

36 36. S. Balendhran, J. Z. Ou, M. Bhaskaran, S. Sriram, S. Ippolito, Z. Vasic, E. Kats, S. Bhargava, S. Zhuiykov and K. Kalantar-zadeh, *Nanoscale*, 2012, **4**, 461-466.

37 37. S. Najmaei, Z. Liu, W. Zhou, X. Zou, G. Shi, S. Lei, B. I. Yakobson, J.-C. Idrobo, P. M. Ajayan and J. Lou, *Nat Mater*, 2013, **12**, 754-759.

38 38. C.-C. Huang, F. Al-Saab, Y. Wang, J.-Y. Ou, J. C. Walker, S. Wang, B. Gholipour, R. E. Simpson and D. W. Hewak, *Nanoscale*, 2014, **6**, 12792-12797.

39 39. Y. Yu, C. Li, Y. Liu, L. Su, Y. Zhang and L. Cao, *Scientific Reports*, 2013, **3**, 1866.

40 40. S. Wu, C. Huang, G. Aivazian, J. S. Ross, D. H. Cobden and X. Xu, *ACS Nano*, 2013, **7**, 2768-2772.

41 41. A. M. van der Zande, P. Y. Huang, D. A. Chenet, T. C. Berkelbach, Y. You, G.-H. Lee, T. F. Heinz, D. R. Reichman, D. A. Muller and J. C. Hone, *Nat Mater*, 2013, **12**, 554-561.

42 42. X. L. Li and Y. D. Li, *Chemistry – A European Journal*, 2003, **9**, 2726-2731.

43 43. K.-K. Liu, W. Zhang, Y.-H. Lee, Y.-C. Lin, M.-T. Chang, C.-Y. Su, C.-S. Chang, H. Li, Y. Shi, H. Zhang, C.-S. Lai and L.-J. Li, *Nano. Lett.*, 2012, **12**, 1538-1544.

44 44. G. L. Frey, R. Tenne, M. J. Matthews, M. S. Dresselhaus and G. Dresselhaus, *Physical Review B*, 1999, **60**, 2883-2892.

45